Control Performance Analysis of Load-Based Testing for Air-Conditioning and Heat Pump Systems: Part I-Control Oriented Simulation Model Development

Jie Ma, Chibuoke Eneh, Dongyang Xi, James E. Braun, W. Travis Horton, Jie Cai[1]

Ray W. Herrick Laboratories Purdue University West Lafayette IN 47906 USA

Abstract

Traditional rating procedures for residential air-conditioning and heat pump (ACHP) systems rely on steady-state testing under fixed indoor and outdoor conditions with component controls overridden. While these methods ensure consistency and comparability, they fail to capture a unit's dynamic behaviors under native control and provide limited insights into an ACHP system's real-world performance. To address these issues, dynamic load-based testing methodologies have been developed and were recently adopted by ACHP rating standards such as AHRI 210/240 in the U.S. and CSA SPE-07 in Canada. The load-based testing approach evaluates an ACHP's performance for realistic operating conditions that includes dynamic interactions between the embedded controller and indoor and outdoor environments. However, challenges remain with respect to testing representativity, controllability, and repeatability, which all relate to the dynamic interplay between the ACHP unit and the testing infrastructure. To facilitate analysis of the dynamics and control performance of a load-based test, this paper presents a control-oriented simulation toolkit that models the dynamics of the five interacting components: the test unit, its embedded controller, a wall-mounted thermostat, a virtual building model, and the psychrometric chamber along with its reconditioning system. A specific application of the analysis toolkit is presented - evaluating the impact of the testing chamber's dynamics on the load-based testing performance. Results show that the current load-based

[1]Corresponding author (cai40@purdue.edu).

testing design with the thermostat placed in the indoor chamber together with the test unit can lead to interactions between the chamber dynamics and the feedback control loop that result in unstable responses which would otherwise be stable in the field. This can lead to mischaracterization of the test ACHP's performance. To address this problem, an alternative configuration is proposed where the thermostat is mounted in a fast responding environment or an emulated thermostat is used, to isolate the chamber dynamics from the control loop.

Keywords: Load-Based Testing, Air Conditioners and Heat Pumps, Performance Rating Standard, Feedback Control Analysis

---

1. INTRODUCTION

Standardized rating procedures exist to ensure that all commercially available equipment are evaluated consistently and in a manner that reflects real-world performance. This is typically achieved by applying standardized testing conditions and measurement protocols across products within the same category. Accurate rating methods not only promote fair competition among manufacturers and encourage the development of energy-efficient technologies, but also enable consumers to make informed decisions when purchasing equipment [1]. Current testing and rating procedures for residential air-conditioning and heat pump (ACHP) systems, as specified in AHRI 210/240 [2], ASHRAE 37 [3], ASHRAE 116 [4], EN 14825 [5], and JIS C9612 [6], are primarily based on steady-state performance tests conducted under fixed indoor and outdoor conditions. During these tests, the test unit's native control algorithms are typically deactivated and component controls such as the compressor and indoor fan speeds are held constant at manufacturer-defined settings, limiting the ability to evaluate a system's dynamic behavior in a real-world setting [7]. During the rating process, standardized metrics such as the Seasonal Energy Efficiency Ratio (SEER) and Heating Seasonal Performance Factor (HSPF) are calculated using steady-state test results assuming idealized controls and supplemented by a degradation factor to account for losses during on-off cycling. Although this approach simplifies the laboratory testing process with reasonable repeatability, it fails to capture the influence of native control on the system performance as they interact with the dynamic thermal environment of a building. As a result, it offers limited insights into actual field performance and provides little incentive for

manufacturers to innovate and optimize control algorithms.

To address the limitations of conventional steady-state testing procedures, a load-based testing methodology has been developed to evaluate the dynamic performance of ACHP systems operating under their native control logic. Unlike steady-state rating tests with control overrides, load-based testing allows the equipment to respond naturally to varying indoor conditions, thereby capturing the influence of the embedded controller, thermostat dynamics, and transient operating conditions. In general, two primary strategies for applying thermal loads in laboratory settings have been documented: the test chamber induced load and the virtual building load (VBL) methods. In the former approach, the reconditioning equipment of the psychrometric chamber—or auxiliary devices such as fan coils or electric heaters—is used to impose a prescribed load on the conditioned space. A well-established example is the load-compensation method, originally proposed by the German regulatory body Bundesanstalt für Materialforschung und -Prüfung (BAM)[8] [9]. Cremaschi and PerezPaez [10] demonstrated the feasibility of this approach by directly controlling heat gains in an indoor test room to emulate building loads. Similarly, Palkowski et al. [11] [12] applied a load-compensation framework to measure the dynamic performance of residential ACHP systems in calorimetric chambers. The VBL approach extends the load-compensation method by introducing a dynamic building emulator into the test framework. In this method, the chamber's reconditioning system adjusts the return-air temperature or humidity to reflect how a real building would respond when the unit's delivered capacity does not match the imposed load. Patil et al. [13] first introduced a load-based testing framework using a virtual building model to generate dynamic indoor load conditions for unitary equipment. This concept was later expanded in subsequent studies [14],[15], [16], culminating in the development of a comprehensive load-based testing methodology for residential ACHPs, which now serves as the foundation of CSA SPE-07 [17]. Cheng et al. [18] and Dhillon et al. [19] demonstrated that load-based testing provides a viable alternative to the AHRI 210/240 steady-state rating procedure by enabling year-round evaluation across cooling and heating seasons while capturing interactions between the ACHP and the conditioned environment. Furthermore, Dhillon et al. [20] directly compared the CSA SPE-07 load-based method against the AHRI 210/240 procedure for a 5-ton variable-speed residential heat pump, reporting substantial differences in seasonal performance ratings between the two approaches.

In response to growing interest in more representative testing methods for residential ACHP systems, several stakeholders encouraged the U.S. Department of Energy (DOE) in 2022 to consider procedures to incoporate load-based testing. Given the challenges associated with mandating full load-based testing as a regulatory standard, AHRI and other key stakeholders (including DOE) supported the development of a simplified load-based testing procedure, known as the Control Verification Procedure (CVP) [21], which was formalized in 2024 as Appendix I of both AHRI 210/240-2024 [2] and AHRI 1600-2024 [22]. The CVP is intended to evaluate whether the override of modulating components for variable-speed ACHPs during regulatory testing is consistent with the system's behavior under its native control. It is also used for variable-speed certification. Since early 2024, the Purdue team has conducted a series of CVP evaluations on four residential split heat pumps from different manufacturers. From these tests, several challenges were identified. Firstly, all tested units exhibited oscillatory and even cyclic responses during the CVP tests. The cyclic operations disturbed the operation of the testing chamber's reconditioning system, leading to chamber temperature fluctuations and failures to meet control tolerances specified in the CVP. Cyclic operations during the intermediate-load interval also led to failures to be certified as variable-speed systems for three out of the four tested heat pumps, all of which have a full variable-speed design. Another primary concern is that repeatability and reproducibility of load-based rating methods are inferior to those achieved with the fixed-speed steady-state tests [20] [23]. Achieving accurate outcomes is particularly challenging when considering the ability to obtain consistent results across different test facilities [24]. Contributing factors include the dynamic response of the test facility, such as the temperature and humidity tracking capability of the chamber's reconditioning system, and sensor delays [25]. Testing accuracy is further affected by the use of communicating thermostats. Mossalaei et al. [26] demonstrated that a unit's dynamic performance can vary substantially when operated with different thermostats, owing to differences in their dynamic responses. Another significant concern is the high test burden. Completing the CVP specified in AHRI 210/240 requires over 10 hours of testing when all tolerances are met, and even longer if any test interval fails to meet tolerance requirements. CSA SPE-07 load-based testing requires a comparable testing duration.

The aforementioned issues are all related to the dynamics of the test heat pump and the testing infrastructure. To better understand the root causes of the various issues and identify potential solutions, this paper presents

a control-oriented simulation toolkit that can facilitate analyses of the dynamics and control performance of a whole load-based testing setup. The simulation tool was built on top of several key interacting components: the virtual building model, the psychrometric chamber's reconditioning system, the test heat pump, its load controller, and the thermostat. A specific application of this control analysis tool is presented for investigating the influence of the testing chamber's dynamics on the ACHP control performance under load-based testing. The analysis results show that the chamber dynamics could destablize the heat pump controller which would otherwise be stable in the field. To address this issue, a modified testing configuration is proposed for potential inclusion in future standards to improve the robustness and representativeness of ACHP load-based testing.

2. LOAD-BASED TESTING OVERVIEW

A load-based testing methodology enables the evaluation of heat pump performance under field-representative conditions within a controlled laboratory environment. Figure 1 presents a typical experimental setup for load-based testing, which consists of a heat pump installed in two side-by-side psychrometric chambers representing the indoor and outdoor environments. The thermostat, typically located in the indoor chamber, senses changes in room temperature and modulates the heat pump's stage or speed to adjust the delivered cooling or heating rate whenever the sensed temperature deviates from the setpoint—just as it would in a real installation. A virtual building model uses the heating or cooling rates of the test unit, obtained from real-time measurements, and a pre-programmed building load model to update the virtual building temperature and humidity conditions, which are then provided as setpoints to the indoor chamber's reconditioning system. The indoor thermal loads can be time-varying dependent on the outdoor and indoor conditions.

A complete load-based test may consist of multiple load intervals. During each test interval, the outdoor chamber conditions are maintained at either fixed setpoints or following pre-programmed ramp-down or ramp-up profiles for temperature and humidity. The indoor chamber conditions are dynamically updated based on the interaction between a virtual building model and the test unit's performance measured in real time. Various studies have explored different virtual building models for load-based testing. The most commonly adopted model, as originally proposed by Patil et al. [13] and

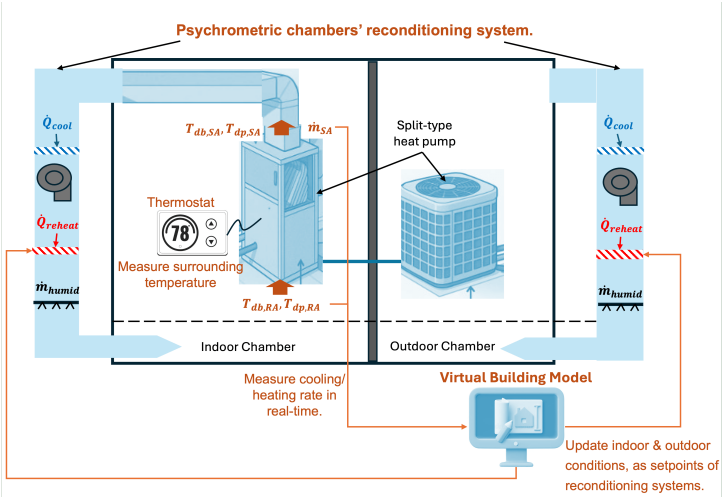

Figure 1: Load-based testing schematic for a split-type heat pump in a psychrometric test facility.

Hjortland and Braun [14], employs a simplified single-node representation of the indoor temperature response based on a sensible energy balance:

$$C_s \frac{dT_{VB,ID}}{dt} = \dot{Q}_{BL,s} - \dot{Q}_s \tag{1}$$

where $T_{VB,ID}$ denotes the virtual building indoor temperature, used as the indoor psychrometric chamber setpoint; $\dot{Q}_s$ is the measured sensible cooling (positive) or heating (negative) rate delivered by the test unit in real time; and $\dot{Q}_{BL,s}$ denotes the emulated sensible building load, expressed as:

$$\dot{Q}_{BL,s} = UA_{BL}(T_{OD} - T_{BAL}) \tag{2}$$

where UA_{BL} is an overall conductance for heat transfer through the envelope termed the building load line conductance, T_{OD} is the outdoor temperature, and T_{BAL} is the balance temperature. The balance temperature is defined as the outdoor temperature at which the net cooling (or heating) load becomes zero after accounting for internal heat gains, and is therefore lower than the indoor temperature.

Currently, two approaches are proposed to determine the building load line conductance and balance temperature. Taking the cooling mode as an example, the method adopted in CSA SPE-07 [17], referred to as the CSA load line, dynamically updates the balance temperature as a function of the

virtual indoor temperature ($T_{VB,ID}$) according to:

$$T_{BAL}(t) = T_{BAL,D} + (T_{VB,ID}(t) - T_{ID,D}) \tag{3}$$

where $T_{BAL,D}$ is the design balance-point outdoor temperature; $T_{ID,D}$ is the test unit thermostat setpoint or the design indoor temperature. The building load line conductance (UA_{BL}) is expressed as:

$$UA_{BL} = \frac{1}{f_{os}} \frac{\dot{Q}_D \cdot SHR_{bld}}{T_{OD,D} - T_{BAL,D}} \tag{4}$$

where $\dot{Q}_D$ and $T_{OD,D}$ denote the total cooling capacity and the outdoor temperature at the design-point operating conditions, respectively, consistent with the A_{full} test conditions specified in AHRI 210/240-2024. SHR_{bld} is the sensible heat ratio of the virtual building; and f_{os} is the oversizing factor.

In an alternative approach presented in Appendix I of AHRI 210/240-2024 [2], the CVP load line is established by two virtual sensible loads: $VL_s(95)$, set to 97% of the sensible capacity from the A_{full} test at an outdoor temperature of 95 °F, and $VL_s(67)$, set to 103% of the sensible capacity from the F_{low} test at an outdoor temperature of 67 °F:

$$\begin{aligned} VL_s(95) &= 0.97 \cdot \dot{Q}_{A_{full},s} \\ VL_s(67) &= 1.03 \cdot \dot{Q}_{F_{low},s}. \end{aligned} \tag{5}$$

In this approach, the balance temperature (T_{BAL}) is fixed at the design value ($T_{BAL,D}$), obtained by extrapolating the load line to its zero-load intercept, as defined below:

$$T_{BAL}(t) = T_{BAL,D} = 95 - \frac{VL_s(95)}{(UA)_{BL}} \tag{6}$$

where UA_{BL} is expressed as:

$$UA_{BL} = \frac{VL_s(95) - VL_s(67)}{95 - 67} \tag{7}$$

Figure 2 compares the two sensible load lines generated as examples based on the steady-state test results given in Table 1 and parameter values listed in Table 2. The CSA load line is established by the design outdoor temperature of 95 °F, where the sensible load equals the full-load cooling capacity

(A_{full}) multiplied by a design building SHR_{bld} of 0.8, and the design balance outdoor temperature $T_{BAL,D}$ of 67 °F. The CVP load line is constructed from the scaled virtual sensible loads $VL_s(95)$ and $VL_s(67)$, with the design balance outdoor temperature obtained by extrapolating the line to zero load, yielding a value of 51.7 °F. The slope of each load line represents the building load conductance UA_{BL}, where the CSA load line reflects a fixed design-based representation, while the CVP load line incorporates a building thermal conductance dependent on the minimum compressor and fan speed settings of the test heat pump. Further, the CSA load model involves a variable balance temperature or load that changes with the actual virtual indoor temperature, while the CVP model simulates a cooling load that is only dependent on the outdoor temperature with a fixed T_{BAL}. These differences between the two load models lead to different transfer function forms and closed-loop dynamics, to be discussed in later sections.

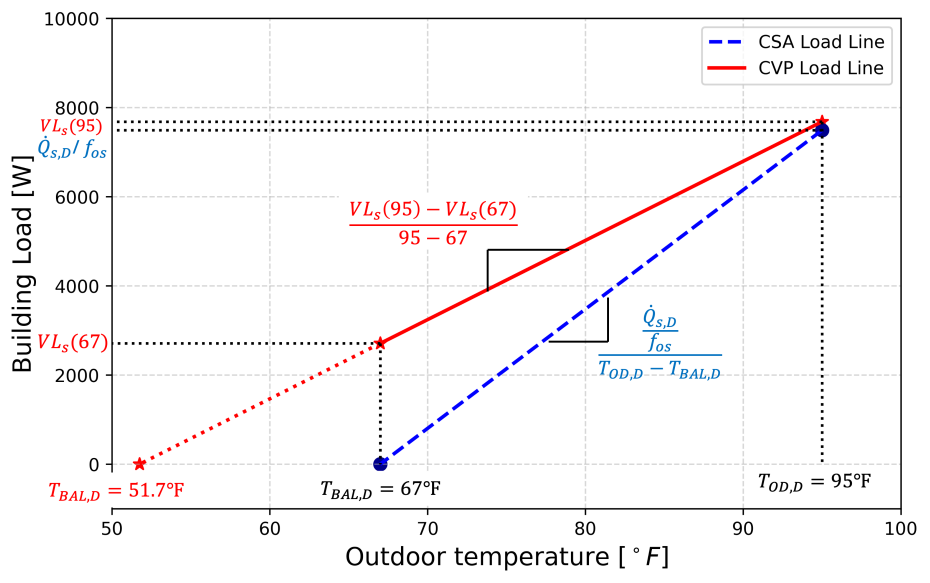

Figure 2: Sensible building cooling load lines for CSA and CVP.

Table 1: Steady-state cooling test performance and component settings.

Tests	**Total Cooling Rate** [W]	**Sensible Cooling Rate** [W]	**SHR** [-]	**Compressor Speed** [RPM]	**Indoor Air Flow** [CFM]
A_{full}	10299	7920	0.769	3550	1150
F_{low}	3117	2603	0.835	1600	650

Table 2: CSA load line parameters.

Parameters	$T_{\mathrm{BAL,D}}$ $[F]$	$\dot{Q}_D$ $[W]$	SHR_{bld} –	f_{os} –
Value	67	10299	0.8	1.1

Both methods discussed above account for the indoor temperature dynamics but differ in their treatment of humidity. CSA SPE-07 models dynamic humidity response within the virtual building, whereas the AHRI 210/240-2024 CVP test fixes the indoor wet-bulb temperature at 67 °F, neglecting transient humidity effects and potentially misrepresenting the latent load on the heat pump.

Figure 3 shows example CVP test results with a 3-ton split heat pump in cooling mode. This heat pump is also used as the test unit for all analyses in this study. Three load intervals representing the full-load, intermediate-load, and minimum-load conditions were tested with outdoor setpoints of 95 °F, 82 °F, and 67 °F, respectively, separated by transition periods with a ramp-down rate of 1 °F per 15 minutes. During the test, a constant indoor thermostat setpoint of 80 °F was used with the manufacturer-provided thermostat on a vertical board within 12 inches from the centerline of the return air vent. The virtual indoor room temperature was updated in accordance with the virtual building model every second. The virtual indoor temperature was sent to the indoor chamber reconditioning system as its setpoint, and the heat pump return air temperature was used as the indoor chamber control temperature. The steady-state test results used to determine $VL_s(95)$ and $VL_s(67)$ are summarized in Table 1. The wet-bulb temperature was maintained at 67 °F for the indoor chamber throughout the test.

The top subplot of Figure 3 presents the virtual building indoor temperature generated by the virtual building model and the return air temperature on the left vertical axis, while the outdoor chamber temperature and its setpoint are shown on the right vertical axis. The lower subplot depicts the unit sensible & latent cooling rates and the virtual building sensible load calculated with the virtual building model on the left vertical axis, and the total outdoor power consumption and indoor fan power on the right vertical axis. Throughout the load-based test, the return air temperature was regulated to track the virtual indoor temperature, within a ±1 °F error band required by CVP. The outdoor room temperature was also well regulated around its

setpoint for most of the test period, although slight deviations outside the tolerance bands were observed due to heater control delays in the chamber reconditioning system and the cyclic operation of the heat pump.

In 2024, the U.S. DOE started requiring the use of the full-load and low-load test results of the CVP to evaluate whether the override settings for the compressor and fan speeds prescribed in regulatory tests are representative of operation under native control. During the full-load test interval, the compressor and indoor fan speeds operated at levels similar to those in the regulatory steady-state A_{full} test where the delivered sensible cooling rate closely matched the virtual building sensible load. This was expected since the full load in the CVP is set to 97% of the sensible cooling rate in the A_{full} test, and the compressor speed is expected to saturate close to the full or nominal speed. In contrast, during the low- and intermediate-load intervals, the unit exhibited cycling behavior, with the compressor bouncing back and forth between full speed and complete shutdown. The indoor fan always operated at full speed whenever there was a cooling call. This cycling behavior led to two issues associated with performance rating: (1) the cooling rate and COP of the test unit during the low-load interval are not consistent with the regulatory F_{low} test results, resulting in failure to meet the U.S. DOE requirements of less than 10% discrepancy in efficiency and less than 6% discrepancy in cooling capacity between the steady-state override and native control [9], and (2) failure to earn a variable-speed certification - CVP requires that the standard deviation of system power remains within 20% of the mean system power during the intermediate-load interval [2].

The team has conducted a series of CVP evaluations on four residential split heat pumps from different manufacturers, and similar cycling control behaviors were observed across all units tested [26]. This cycling behavior is believed to be caused by improperly designed controllers and flaws with the current design of the CVP testing methodology. Load-based testing involves a complicated testing facility with multiple components interacting with each other and the associated controllers. Thus, a simulation toolkit was developed to facilitate analysis and investigation of the root causes for the problematic control behaviors and to identify potential solutions.

3. CONTROL-ORIENTED SIMULATION TOOLKIT

During load-based testing, the dynamic response of an ACHP unit depends on the interactions of different subsystems in a testing infrastructure,

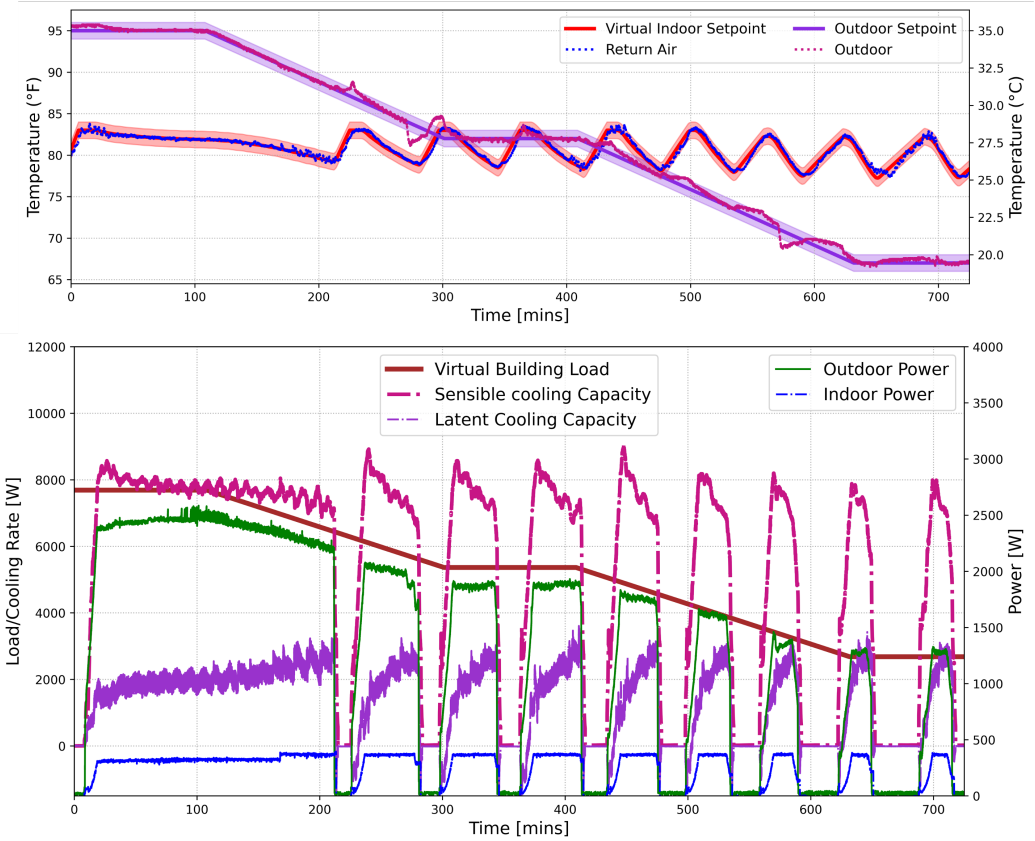

Figure 3: Example CVP test results.

including the test unit and its native controller, the virtual building model used to emulate dynamic responses of the indoor environment, and the psychrometric chambers with their reconditioning systems. Because these components are tightly coupled, it is often difficult to isolate individual factors or components that cause unstable or unsatisfactory control performances. To investigate the overall system dynamics and control performance, a control-oriented simulation toolkit was developed that captures the dynamics and interactions of the following five major subsystems: the test unit, the load controller of the unit, the virtual building model, the thermostat, and the psychrometric chambers. A high-level control diagram of the overall system is shown in Figure 4, while individual blocks may involve lower-level feedback controllers to be detailed in the following subsections. In this outermost control loop, the thermostat control error, i.e., the difference between the

thermostat temperature reading and its setpoint, is used by the heat pump load controller to determine the compressor and fan speeds. The resulting cooling or heating rate supplied by the unit is fed to the virtual building model to emulate the dynamic response of the indoor environment. The indoor temperature and humidity predicted by the virtual building model are then imposed as the setpoints of the indoor chamber controller, which modulates the psychrometric chamber reconditioning system to track the references. The thermostat installed in the indoor chamber measures the chamber air temperature, providing a feedback signal to be used by the heat pump controller along with its setpoint for capacity control.

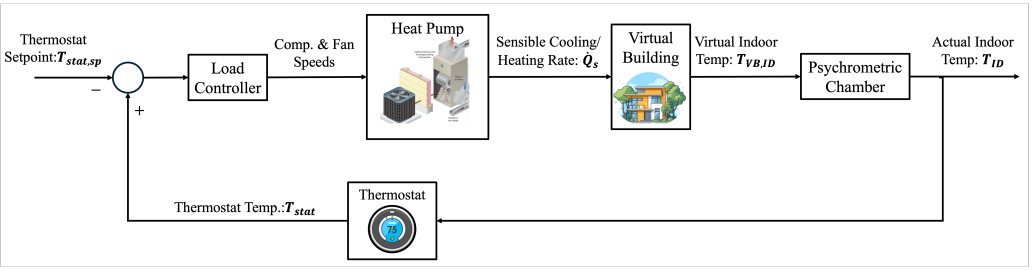

Figure 4: Control diagram of the load-based testing methodology.

3.1. Variable-Speed Heat Pump

Unlike traditional fixed-speed units, which cycle on and off to meet indoor thermal loads, variable-speed heat pumps incorporate modulating compressors, fans, and expansion devices that allow continuous capacity adjustment. This capability allows the system to better track instantaneous building loads, thereby reducing cycling losses, improving part-load efficiency, and maintaining more stable indoor temperature control when a properly designed controller is in place.

A variable-speed heat pump is typically operated with two separate controllers:(1) a capacity or load controller that determines the required cooling or heating capacity based on deviations of the sensed indoor temperature from its setpoint, and (2) a superheat controller that modulates the electronic expansion valve (EXV) to maintain a desired evaporator outlet superheat, as shown in Figure 5. The capacity controller also translates the percentage cooling or heating request to the compressor and fan speed commands sent to the respective components to execute.

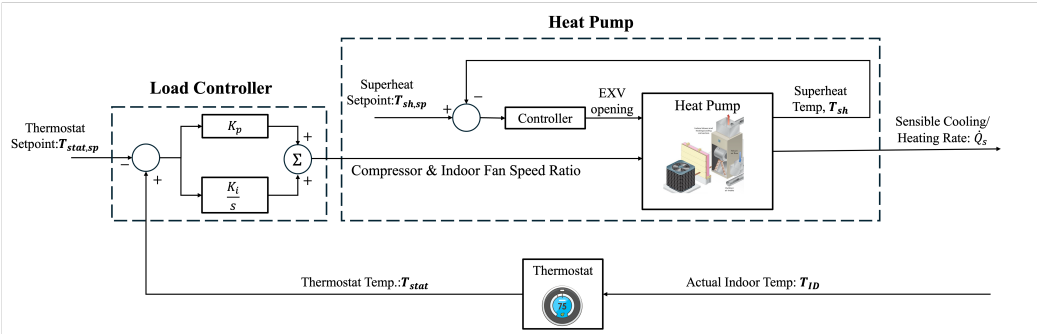

Figure 5: Control diagram for a heat pump and its load controller

To facilitate control testing, the team gained full control access to the major components of the test heat pump through a proprietary communication protocol provided by the manufacturer. Custom capacity and superheat controllers were programmed in a National Instruments CRIO controller through LabVIEW. Liu et al. [27] conducted a thorough stability analysis for the superheat controller, and the developed proportional–integral (PI) controller was adopted in this study. For capacity control, the compressor and indoor fan speeds are synchronized - the percentage cooling or heating request is linearly projected to the compressor and fan speeds. The operating ranges of the compressor and indoor fan speeds were determined from the steady-state tests at the A_{full} and F_{low} conditions specified in AHRI 210/240-2024 and are summarized in Table 1. When the compressor speed reaches the minimum and the thermostat temperature stays below the lower deadband for a duration of 3 minutes, the heat pump is shut down. Similarly, when the compressor speed saturates at its maximum and the thermostat temperature stays above the upper deadband for a duration of 3 minutes, the heat pump is turned back on, where capacity modulation is re-engaged starting at the minimum speed.

Since the compressor and indoor fan speeds are synchronized, the heat pump system dynamics can be characterized by a single-input–single-output (SISO) model. To evaluate the dynamics of the test heat pump, step response tests were conducted by applying step changes in the speed ratio from the minimum to three different settings that cover the heat pump dynamics at different load levels. During each test, the EXV was maintained at a fixed position to ensure the observed variations in the cooling rate were solely attributed to changes in the compressor and fan speeds. A first-order linear

time-invariant model was then identified using the obtained step response test results, in the following form:

$$G_{hp}(s) = \frac{\dot{Q}_{cooling}(s)}{\delta(s)} = \frac{K_{hp}}{\tau_{hp}s + 1} \tag{8}$$

where K_{hp} is the static gain and τ_{hp} is the time constant of the heat pump model; these are the two main model parameters estimated by minimizing the error between the model prediction and the experimental results. The model accepts the speed ratio (δ in %) as the input and outputs the sensible cooling capacity in W. It should be noted that the sensible cooling rate delivered by the heat pump has a nonlinear dependence on the compressor and indoor fan speeds. However, for control stability analysis within a specific range of operating conditions, linear approximate models are reasonably accurate and more suitable.

Figure 6 compares the measured and simulated sensible cooling rate for the three step response tests. The plotted sensible cooling rate has the minimum sensible capacity subtracted, and the step changes are aligned in the time axis to afford a better comparison. The identified static gain is $K_{hp} = 84.24$ (W/%) and time constant is $\tau_{hp} = 20$ (s). The heat pump has the fastest dynamics compared to the other components to be discussed in later sections. Note that the superheat control loop is not modeled in this study, because the refrigerant superheat dynamics are even faster than the air-side capacity response and their impact on the overall system stability is believed to be small.

3.2. Load Controller

A heat pump's capacity or load controller uses the error between the thermostat temperature and its setpoint to determine the compressor and fan speed ratio for the heat pump to meet the load. A PI controller is considered in this study:

$$C(s) = K_{p,hp} + \frac{K_{i,hp}}{s} \tag{9}$$

where $K_{p,hp}$ and $K_{i,hp}$ denote the proportional and integral gains, which are set to 140.84 (%/°F) and 0.00845 (%/°F-s), respectively, based on work presented in the companion paper [28]. A more thorough control design analysis is presented in the companion work along with a proposed higher-order controller to achieve improved performance.

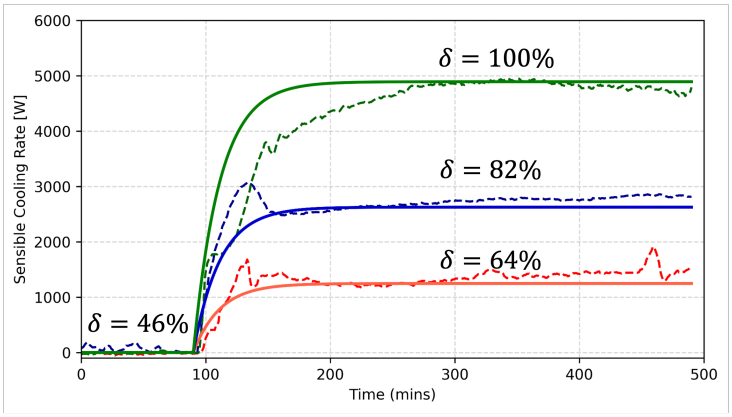

Figure 6: Step response test results of haet pump.

3.3. Thermostat

A thermostat senses the indoor environmental conditions and feeds the measurements to the heat pump controller for capacity control. The dynamics of a thermostat are impacted by multiple factors, including sensor location, thermal inertia of the enclosure, ventilation design, surrounding airflow, and internal signal filtering. These features can influence the response of the temperature signal provided to the heat pump, thereby affecting a heat pump's overall control performance. A thermostat with a slow response can pose challenges for controller design, whereas a thermostat with a fast response may induce short cycling of the heat pump at low load conditions.

In this study, dynamics of five thermostats from different mainstream manufacturers were characterized through laboratory tests. As shown in Figure 7, the five thermostats were mounted on a common board, with two thermocouples positioned at the top of the mounting board to provide reference temperature measurements. The board was first placed in an environment with a stable temperature at 70°F and was kept there until the temperature readings from the display of each thermostat stabilized. For thermostats with temperature readings different than 70°F, an offset was applied to the thermostat temperature during postprocessing. The board was then quickly moved to another psychrometric chamber maintained at 76°F. This move subjected each thermostat to a sudden step change in the ambient temperature. Since the measured temperature from the thermostats could not be accessed directly, a camera was positioned in front of the thermostats to tape record the temperature displayed throughout the test. The recorded video

was then postprocessed with an optical character recognition (OCR) algorithm [29] to extract the displayed temperatures as time-series data, which were subsequently aligned with the reference thermocouple measurements to evaluate the dynamic response of each thermostat.

Figure 7: Thermostat dynamic test setup.

The time-series temperature data collected was utilized to develop a first-order model for each thermostat. The DC gain and time constant were estimated from the test data. Figure 8 presents the measured and simulated step responses for the five thermostats (#1 – #5), and the estimated time constants, denoted as τ, are reported alongside each curve. Upon a step change in the environment temperature, the thermocouple readings changed almost instantaneously. In contrast, all five thermostats approached the new temperature at much slower rates. Four out of the five thermostats have a temperature resolution of 1 °F and thermostat #4 has a resolution of 0.1 °F. Because of that, all the thermostat readings exhibited staircase-shaped trajectories (shown as dashed lines in Figure 8), rather than smooth curves. The fitted first-order models (solid curves in Figure 8) show good agreement with the thermostat temperature responses. Thermostats #1 through #4 exhibited comparable response times, whereas thermostat #5 responded at a slower pace, with an estimated time constant of 1333 s. Despite this difference, the five thermostats showed very similar dynamics.

For subsequent analyses, a representative time constant of 1200 s was adopted, which is close to the average across the five thermostats. Thermostats #1 through #4 involve static gains higher than unity and thermostat #5 has a static gain close to unity. The higher temperature measurements by the four thermostats could be driven by the heat generated by the electronics inside the thermostats. To simplify the analysis, a unity static gain was assumed for the thermostat model. The final transfer function for the

thermostat is

$$G_{stat}(s) = \frac{1}{1200s + 1}. \tag{10}$$

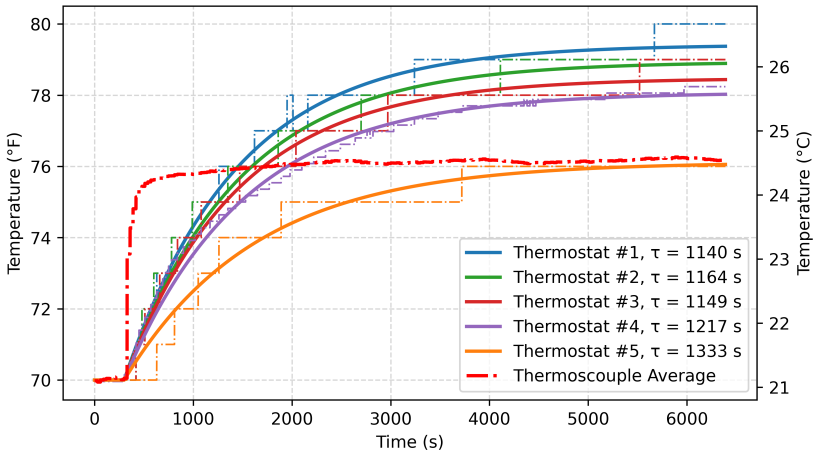

Figure 8: Thermostat step response test results.

3.4. Virtual Building Model

The virtual building model is treated as an individual subsystem, allowing flexibility to examine the influence of different virtual load models on the heat pump control performance. As illustrated in Figure 9, the virtual building model relates the controllable input—the sensible cooling rate measured in real time off the test unit in W—to the virtual building indoor temperature in °F. External disturbances such as the ambient temperature and internal heat gains also affect the indoor temperature, but such disturbance effects do not influence the main loop dynamics and thereby are not included in the model.

Following the discussions in Section 2, two distinct building load models are considered, namely, the CSA and the CVP load models. For the CSA load model in cooling mode, Laplace transforming Equations 1 to 3 yields the following transfer function between the virtual indoor temperature and sensible cooling rate:

$$G_{VB}(s) = \frac{T_{VB,ID}(s)}{\dot{Q}_{c,s}(s)} = -\frac{1}{C_s s + UA_{BL}} \tag{11}$$

where the design balance outdoor temperature $T_{BAL,D}$, design indoor temperature $T_{ID,D}$ and outdoor temperature T_{OD} in Equation 1 are treated as external disturbances (d_{VB}) for the control analysis and therefore are not present in the above equation. Based on the test results in Table 1 and parameter values in Table 2, $UA_{BL} = 267.5$ W/°F (0.254 Btu/(s · °F)) and $C_s = 1.234 \times 10^6$W· s/°F (1170Btu/°F) for the CSA model. The CSA load model involves a time constant of 4621 s, which represents the slowest dynamics among all the subsystems considered.

Similarly, applying the Laplace transform to the CVP load model shown in Equations 1, 2, and 6 leads to the following transfer function:

$$G_{VB}(s) = \frac{T_{VB,ID}(s)}{\dot{Q}_{c,s}(s)} = -\frac{1}{C_s s} \tag{12}$$

where $\dot{Q}_{BL,s}$ is treated as the external disturbance (d_{VB}) and C_s assumes a value of 1.187×10^6W· s/°F (1125Btu/°F) in the CVP load model.

The CSA load model has a standard first-order form with a stable real pole at $-UA_{BL}/C_s$, while the CVP model is essentially an integrator. This difference can affect the control design and analysis in several ways: (1) the integrator in the CVP load model reduces the phase margin at low frequency ranges and can cause control oscillations and even instability for a slow responding controller; (2) integral actions are needed to eliminate steady-state errors when tested with the CSA load model, while for the CVP load model, no additional integral components are needed; (3) for fast responding controllers, there is negligible difference in the closed-loop response between the two models. A more in-depth analysis of the virtual load model impact can be found in the companion paper [28].

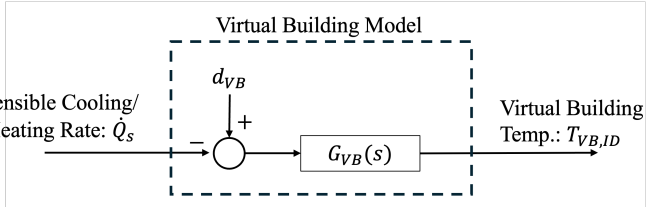

Figure 9: Control schematic diagram of the virtual building model

3.5. Psychrometric Chamber

Performance rating of heat pumps heavily relies on psychrometric chambers that can provide accurately controlled temperature and humidity con-

ditions to simulate different outdoor and indoor environments to study the performance and behavior of the test equipment. The chamber's psychrometric conditioning unit (PCU) provides a counteracting thermal input to offset the heating or cooling effects produced by the test equipment, as well as those associated with air leakage and other incidental loads. A humidity control subsystem can also be employed to manage latent loads [30].

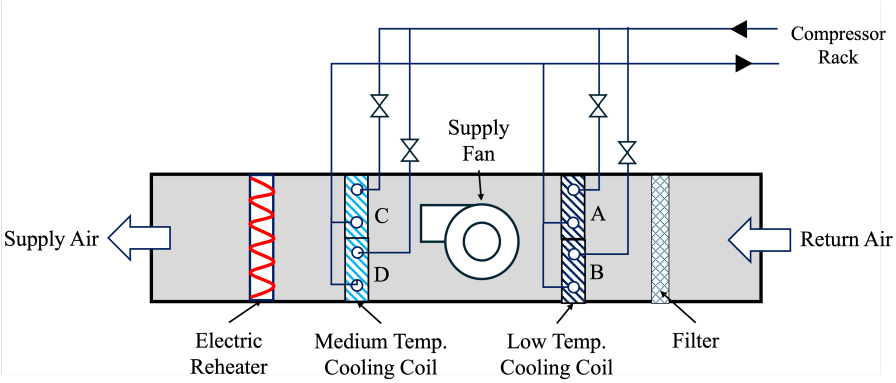

Figure 10: Psychrometric conditioning unit (PCU) configuration.

The test unit used in this study was installed in the psychrometric chambers at Ray W. Herrick Laboratories at Purdue University. Unlike the conventional steady-state performance rating method where the chamber conditions are held constant for each test point, load-based testing requires dynamic adjustment of the indoor environmental conditions to simulate the interaction of the heat pump with the indoor and outdoor environments. Therefore, characterization of the chamber dynamics is critical for the control stability analysis for a load-based test. In this study, only the dry-bulb temperature dynamics of the psychrometric chambers are considered. This would allow control analysis of the CVP directly, which involves a constant wet-bulb temperature for both the indoor and outdoor environments. The PCU used for temperature control is shown schematically in Figure 10, which incorporates four cooling coils located upstream of an electric reheat section, arranged in two temperature banks: Coils A and B form the low-temperature bank, and Coils C and D form the medium-temperature bank. All four coils are connected to a compressor rack comprising one medium-temperature compressor (serving Coils C and D) and two low-temperature compressors (serving Coils A and B). This arrangement provides sufficient

turndown and flexibility to accommodate a wide range of experimental conditions. During operation, either the medium- or low-temperature coil bank is enabled, and either one or both coils can be operated in the active bank to stage the capacity based on the chamber's cooling demand.

For chamber temperature regulation, the return air to the PCU is first over-cooled by the direct-expansion (DX) coils, after which a PI-controlled electric reheat unit restores the supply air to the desired condition. The suction temperature of the activated coils is maintained at a given setpoint through capacity modulation of digital scroll compressors. This ensures an approximately constant coil surface temperature across tests. The supply fan speed is held constant during operation, so that airflow through the PCU also remains constant. This design ensures a relatively constant cooling effect provided by the DX coils, while a solid-state relay-controlled electric heater is employed for fast load matching. These measures isolate the DX coil dynamics from the chamber response, allowing for more accurate and faster temperature regulation.

The control architecture of the psychrometric chamber is shown in Figure 11. A PI controller is used to modulate the electric heat output in response to the deviation of the measured chamber temperature from its setpoint. The cooling effect of the DX coil banks and other thermal loads, including the cooling or heating effect generated by the test heat pump, are lumped into a single disturbance input, denoted by d_{chb} in Figure 11.

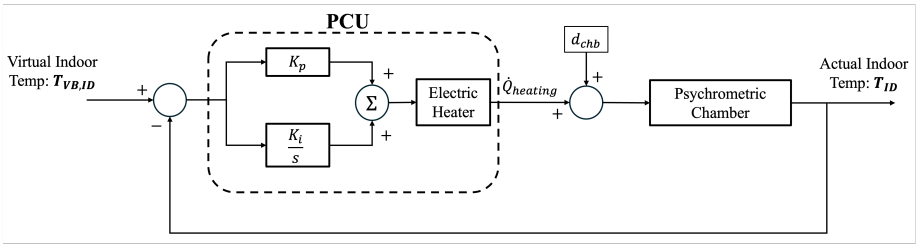

Figure 11: Control block diagram of the psychrometric chamber.

To identify a dynamic model for the psychrometric chamber testing facility, a closed-loop step response test was conducted. In this test, the medium-temperature coils (Coil C and Coil D) were activated, and the coil suction temperature was set at 35 °F, with the PCU supply fan operating at its maximum speed. These represent the typical settings for the indoor chamber used for load-based testing. The test started with an initial chamber temperature

setpoint of 83 °F, followed by a step change to 81 °F. The closed-loop transfer function for the combined dynamics of the psychrometric chamber, electric heater, and its PI controller is given by:

$$G_{chb}(s) = \frac{\left(K_{p,chb} + \frac{K_{i,chb}}{s}\right)\frac{K_{chb}}{\tau_{chb}s+1}}{1+\left(K_p + \frac{K_{i,chb}}{s}\right)\frac{K_{chb}}{\tau_{chb}s+1}} = \frac{K_{chb}K_{p,chb}s + K_{chb}K_{i,chb}}{\tau_{chb}s^2 + (K_{chb}K_{p,chb}+1)\,s + K_{chb}K_{i,chb}} \tag{13}$$

where $K_{p,chb} = 10$ (%/°F) and $K_{i,chb} = 0.0165$ (%/°F-s) are the proportional and integral gains of the PCU heater controller. These gains were fine-tuned and showed satisfactory control performance over the past 10 years of work on load-based testing. A first-order dynamic model was assumed to characterize the dynamics between the heater control command and the chamber temperature, where τ_{chb} is the time constant, with an estimated value of 3755 s, and K_{chb} is the DC gain, with an estimated value of 2.85 (°F/%).

Figure 11 compares the measured and simulated dynamic closed-loop responses of the psychrometric chamber. The model was able to predict the closed-loop dynamics of the chamber testing facility with reasonable accuracy. The identified chamber system model has two negative real poles with a time constant of 450 s for the dominant pole, leading to a response slower than the heat pump, but faster than the thermostat.

3.6. Integrated System Model

The disparate subsystem models presented above were integrated to establish a complete system model to facilitate control design and performance analysis. The overall closed-loop system transfer function that relates a thermostat temperature to its setpoint is given in Equation 14. The model was implemented in MATLAB and the Control System Toolbox was used for some of the analyses presented in this study.

$$G_{sys} = \frac{C \cdot G_{hp} \cdot G_{VB} \cdot G_{chb} \cdot G_{stat}}{C \cdot G_{hp} \cdot G_{VB} \cdot G_{chb} \cdot G_{stat} - 1} \tag{14}$$

4. APPLICATION OF SIMULATION TOOLKIT

The simulation toolkit developed in this study can be applied to investigate different control issues in load-based testing and support heat pump

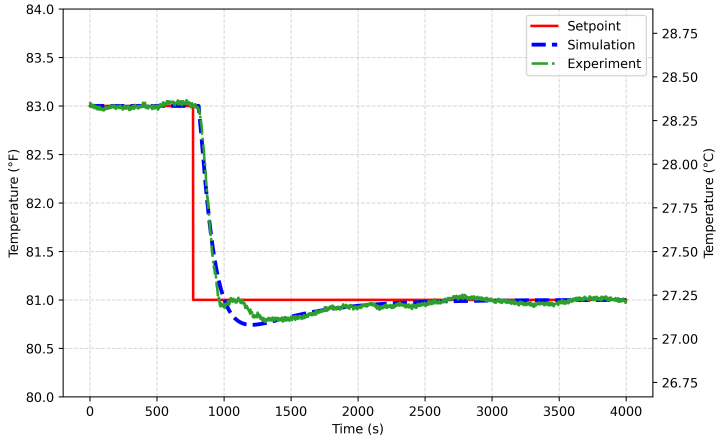

Figure 12: Step response test results of the psychrometric chamber.

controller design in a more general setting. In this section, a specific application of the simulation tool is presented - evaluation of the impact of psychrometric chamber dynamics on the heat pump control performance.

In the current design of the CVP, the thermostat is located within and is exposed to the conditions of the indoor psychrometric chamber. Very often, the return air temperature (RAT) measurement is used as a proxy for indoor chamber environmental control, as it is exactly what the indoor unit sees. This configuration, referred to as the RAT case, loops in the slow dynamics of the chamber environmental control system during load-based testing, which are not present in a heat pump's field operation. Therefore, the performance assessment using the load-based testing approach may not capture the actual field performance. That is why it is important to understand the impact of the testing facility's dynamics on the heat pump control behaviors and performance.

To this end, an alternative configuration is proposed as shown in Figure 13, where the indoor temperature generated by the virtual building model—referred to as the virtual building temperature (VBT)—is directly fed to the thermostat model as its ambient temperature. This configuration, referred to as the VBT case, eliminates the influence of chamber dynamics on the control loop and thus can better represent a heat pump's field performance. This VBT configuration can be implemented either with an emulated thermostat (the case for this study) or by placing the thermostat in a thermostat environment emulator (TEE) [31] [32], which has a much

faster response compared to a full psychrometric chamber.

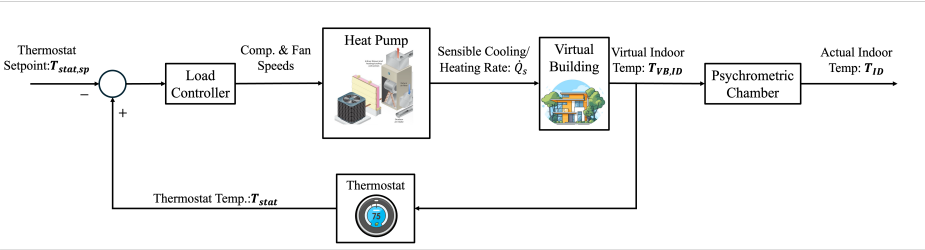

Figure 13: Control diagrams for the VBT testing configuration.

4.1. Control Stability Analysis

Figure 14 compares the closed-loop pole and zero locations for the RAT and VBT configurations. The closed-loop zeros are marked as circles and the pole locations are highlighted by the cross markers. It can be observed that the closed-loop response is unstable with a pair of complex poles on the right half plane for the RAT case, caused by the slow chamber dynamics, while stable control is achieved for the VBT case. Although stable, the VBT case involves a dominant pole close to the imaginary axis. However, there is a closed-loop zero very close to it that can almost cancel the effect. Such imperfect zero-pole cancellation near the imaginary axis results in slow "residual dynamics" - the temperature settles within a small band around the setpoint relatively fast, but it takes a long time for the small error to die out. The slow "residual dynamics" can be easily spotted in the simulation results presented in the following subsection. With the "imperfect" zero-pole cancellation, the complex poles play a dominant role in the closed-loop dynamics for the RAT case. However, they are still close to the imaginary axis, resulting in a small phase margin. As a result, oscillatory responses are expected.

4.2. Simulation Results

The RAT and VBT cases were simulated using the developed simulation test bed. The discrepancy between the simulation results reveals the impact of the chamber dynamics on the heat pump closed-loop response. A test sequence was designed consisting of two consecutive segments:

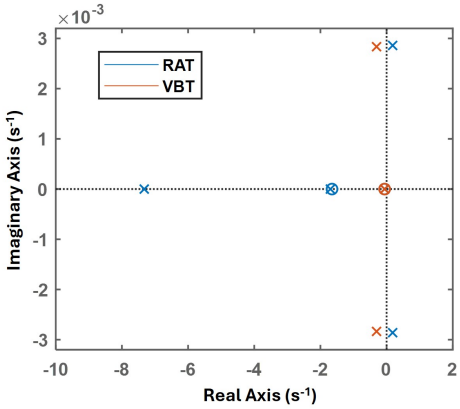

Figure 14: Closed-loop zero and plot locations for the RAT and VBT cases.

- Segment 1: the test starts at the full-load conditions defined in the CVP and the load is then gradually reduced to the intermediate level, with the thermostat setpoint fixed at 73°F;
- Segment 2: the thermostat setpoint steps up from 73°F to 75°F while the sensible load is held constant at the intermediate level, emulating setpoint step changes in buildings, e.g., during transitions between occupied and unoccupied modes.

The first segment of the test sequence, which consists of the high- and intermediate-load intervals of the CVP, aims to assess the ability of the heat pump controller to track load variations and regulate indoor temperature. The second segment is designed to evaluate the setpoint tracking performance of the controller, which is equally important to load tracking, but is not assessed with the current CVP. It should be noted that the test sequence is only intended to enable comparisons of control behaviors between the RAT and VBT cases under load-based testing.

Figure 15 presents the simulated temperature response and cooling capacity for the RAT case. The upper subplot shows the thermostat setpoint ($T_{stat,sp}$), thermostat temperature (T_{stat}), and the VBT generated by the virtual building model ($T_{VB,ID}$), while the lower subplot depicts the unit sensible cooling rate alongside the virtual building sensible load. The blue shaded period highlights the first segment, while the orange shaded period corresponds to Segment #2. The system exhibited unstable, bang-bang control behaviors across both segments; the compressor and fan oscillated between

the maximum and minimum speeds, which in turn caused fluctuations in the indoor temperature. The zone air temperature fluctuated between 74 °F and 76 °F and failed to stabilize at the new setpoint. In this simulation test, the cycling logic was disabled to afford better comparisons.

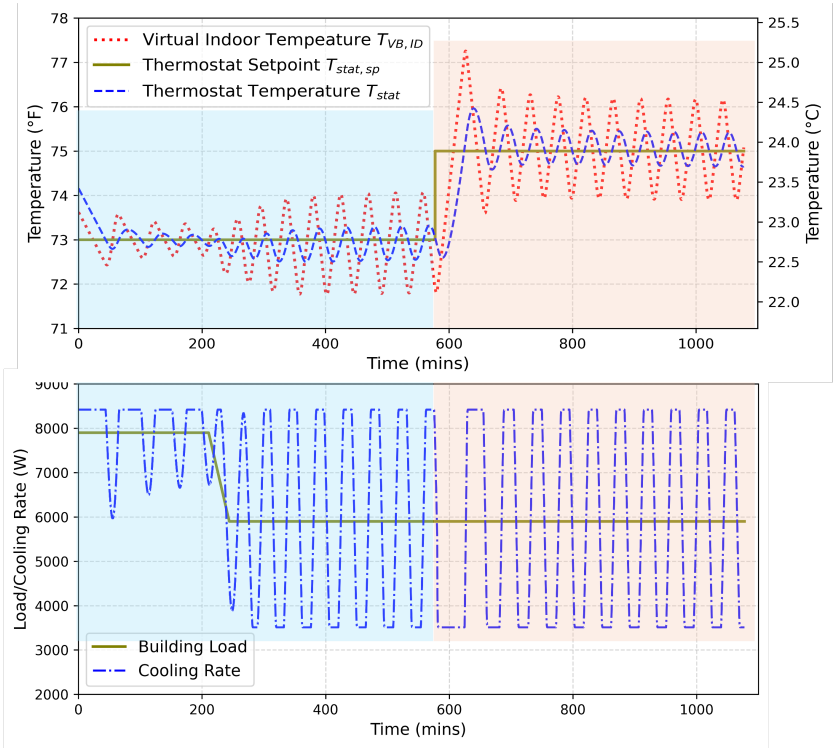

Figure 15: Simulation test results for the RAT case.

Figure 16 presents the simulated temperature response and cooling capacity for the VBT case. At full-load, the control speed fluctuated in the beginning, but the oscillation died out toward the end of the full-load interval. As the test transitioned from the full-load to the intermediate-load interval, the delivered cooling capacity converged to and eventually settled at the intermediate load after a few oscillations. During this load transition, the virtual indoor temperature ($T_{VB,ID}$) exhibited a slight fluctuation of approximately 0.5 °F but stabilized within 10 minutes. The slow residual dynamics caused by the close zero-pole pair can be observed after the load transition, where the small temperature error declined to zero at a very slow rate. At the beginning of the second segment, the unit exhibited a dynamic

response comparable to the RAT case. The delivered cooling rate initially overshooted, and the indoor temperature rose above the new setpoint by approximately 1 °F. Unlike the RAT case, however, the thermostat in the VBT case responded more quickly to the setpoint change and eventually settled at the new setpoint. The controller resulted in stable responses for the VBT case with faster setpoint tracking, compared to the RAT case.

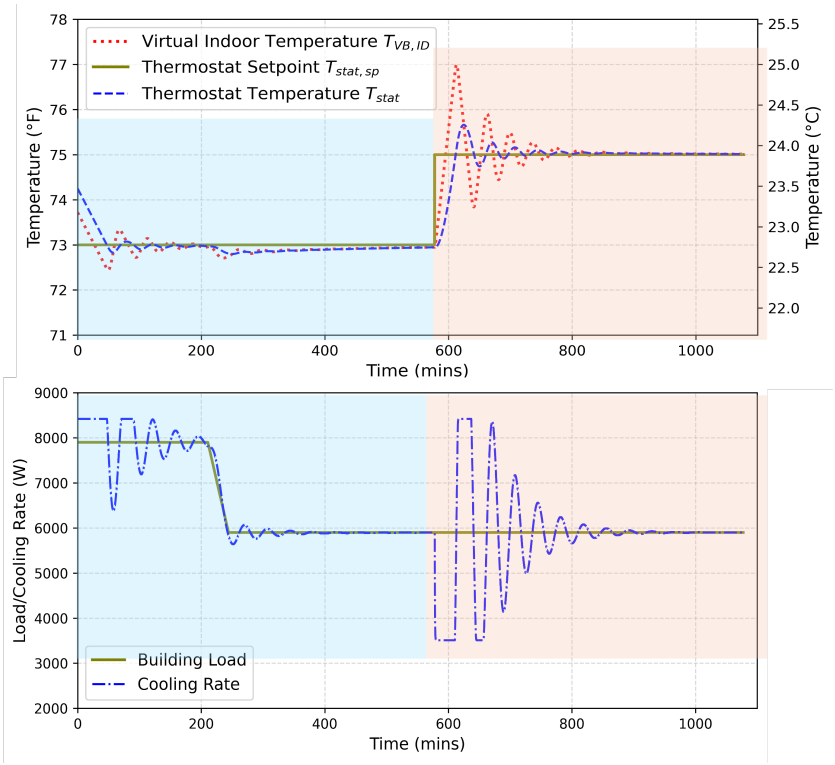

Figure 16: Simulation test results for the VBT case.

4.3. Experimental Results

The simulation study led to a conclusion that the chamber dynamics can destabilize a heat pump controller that may otherwise be stable in the field. To further verify this, experiments were conducted at Herrick Labs for the RAT and VBT cases, with the heat pump discussed in Section 3.1. To facilitate comparative tests, the original thermostat was replaced by a load controller presented in Section 3.2 , along with a thermostat emulator based

on the model introduced in Section 3.3. Both the load controller and thermostat emulator were programmed in the NI CRIO controller. The determined control actions, namely, the compressor and fan speeds, were sent to the heat pump to execute through the manufacturer-provided communication protocol. Tests were only conducted for the intermediate load conditions.

Figure 17 displays the experimental results of the CVP test under the intermediate load for the RAT case. The thermostat temperature oscillated within 0.1 °F around the setpoint, while the virtual indoor temperature fluctuated in a wider range. The actual RAT underwent a more significant and high-frequency fluctuation around the virtual indoor temperature, but the measured temperature by the thermostat was smoother due to its low-pass filtering effect. While the temperature fluctuation still fell within the CVP tolerance, the oscillating control error seen by the controller led to highly fluctuating control actions by the compressor and indoor blower. The oscillations did not die out over the 4-hour test period, alluding to an unstable (marginally stable) control response for the RAT case.

The test was repeated under the VBT configuration against the same intermediate load conditions. The test results are shown in Figure 18. It can be observed that the system stabilized and settled at a steady state after approximately two and a half hours. In this case, the VBT was assumed to be the environmental temperature around the thermostat, which has a faster and smoother response compared to the RAT. The RAT tracked the VBT with reasonable accuracy. However, there was a slight phase shift between the VBT and RAT, caused by the dynamics of the chamber's environmental control system, which led to different control behaviors between the VBT and RAT cases.

To allow better visualization of the impact, simulation tests were conducted by feeding the experimental VBT and RAT, presented in Figure 17 for the RAT case, to the thermostat model. These tests applied a low-pass filter (thermostat model) to the noisy RAT and VBT measurements to obtain smoothed thermostat temperature profiles that can be better compared. Figure 19 shows the simulation test results. It is evident that the thermostat temperature under the RAT scenario (red trend line) has a clear phase lag when compared with that for the VBT case (blue trend line). This phase shift in the control temperature translated to lags in the PI control actions, leading to unstable closed-loop responses.

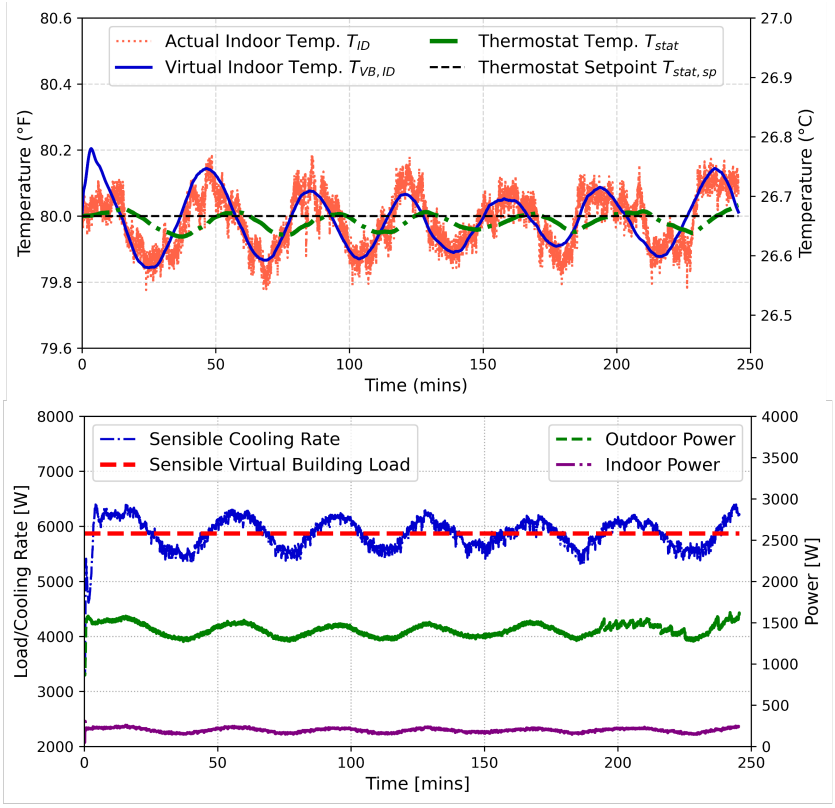

Figure 17: Experimental intermediate load test results for the RAT case.

5. Conclusion

This paper presented a control-oriented, linearized simulation toolkit for control analysis and performance assessment of variable-speed heat pumps under load-based testing. The simulation tool characterizes the overall system dynamics through a feedback loop comprising five key subsystems: thermostat, load controller, test heat pump, virtual building model, and psychrometric chamber. The transfer function for each subsystem was derived from experimental test results, except for the virtual building model, for which the transfer function is directly available from the model's input-output differential equation. Findings were made during the development of this simulation tool:

- A heat pump's dynamics are the fastest among all the subsystems considered. Their impact on the overall control behavior is negligible.

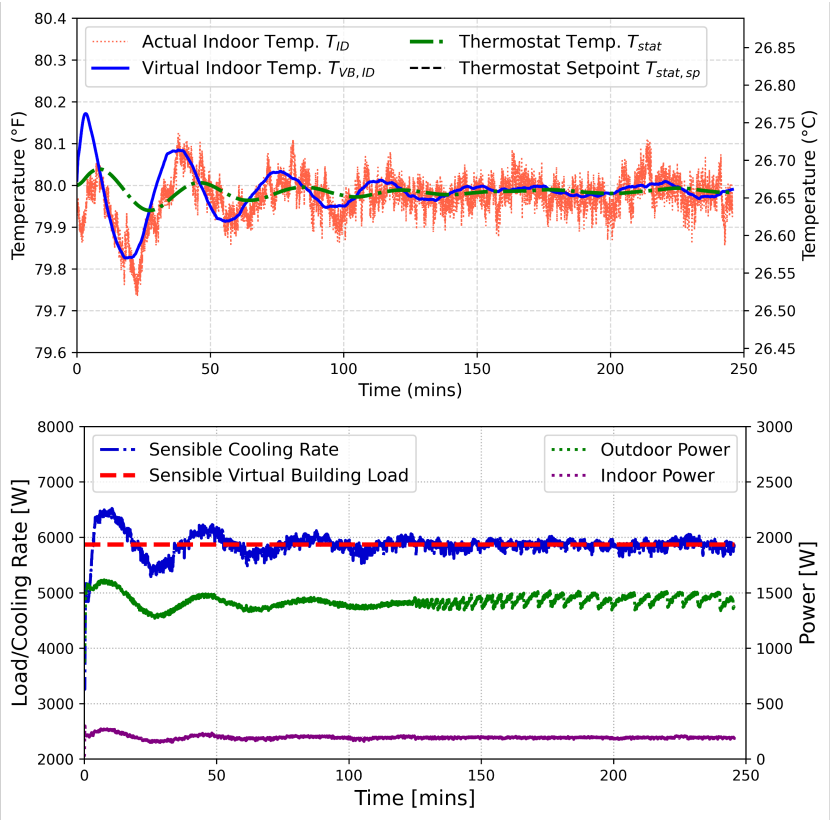

Figure 18: Testing results using VBT as thermostat input.

- Thermostats from different manufacturers appeared to have very similar dynamics, which are much slower than the heat pump and chamber dynamics.

- The psychrometric chamber's dynamics, although not the slowest, still play an important role in the load-based testing performance. Note that the chambers at Herrick Labs, equipped with oversized electric heaters and refrigeration racks, already have fast responses relative to other testing facilities. Diversity in the design of the testing facilities may affect the reproducibility of load-based testing results.

The developed simulation toolkit was applied to evaluate the impact of psychrometric chamber dynamics on the control performance of the test heat pump. Simulation test results show that when the thermostat was exposed

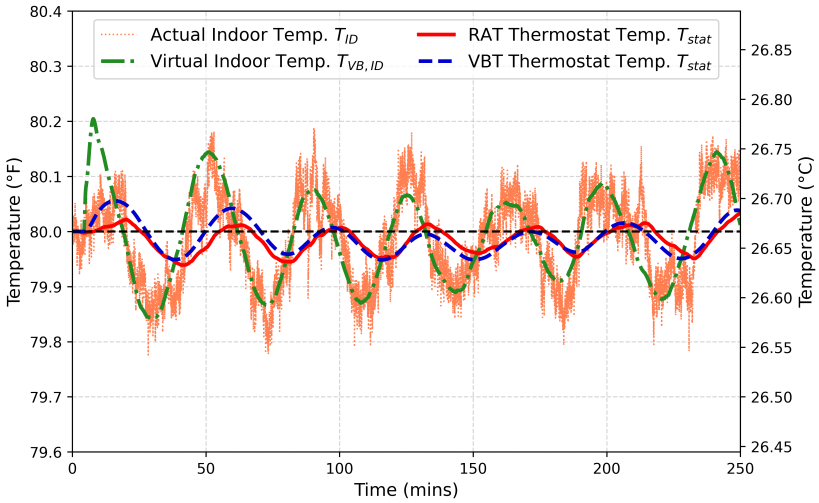

Figure 19: Comparison of thermostat temperature with RAT and VBT temperature feeds.

to the indoor chamber conditions, the slow dynamics of the chamber's environmental control system were introduced into the feedback loop during load-based testing, causing unstable responses of a controller that would otherwise be stable when operated in the field. This conclusion was also verified through experimental tests in psychrometric chambers under two configurations - the first case feeds the measured indoor chamber temperature to the emulated thermostat, and the second case assumes the thermostat emulator takes the virtual indoor temperature as its input. Under the first configuration, a PI controller led to unstable responses, while the same controller was stable under the second configuration. The experimental tests showed consistent behaviors seen in the simulation test results, supporting the conclusion that load-based testing conducted in slow responding psychrometric chambers may mischaracterize a heat pump's field performance. Suggested remedies include: (1) accelerating the dynamic response of the psychrometric chamber's reconditioning system, (2) conducting load-based testing with the thermostat placed in a fast responding environment such as a TEE, and (3) testing a heat pump with an emulated thermostat but using the virtual building temperature as the environment input to the thermostat model instead of the measured indoor chamber temperature.

The control simulation and analysis toolkit developed in this study can support control analysis and design for load-based testing and also in a more

general setting. In a companion paper, this toolkit was used in the analysis and design of controllers for load-based testing that achieve much faster and more stable responses with boosted phase margins [28]. The control implications of the different virtual load models were also studied through both simulation and experimental tests.

CRediT authorship contribution statement

Jie Ma: Writing – original draft, Investigation, Validation; Chibuoke Eneh: Writing – review editing, Investigation; Dongyang Xi: Formal analysis; James E. Braun: Writing – review editing, Supervision; W. Travis Horton: Writing – review editing, Supervision; Jie Cai: Writing – review editing, Supervision, Methodology, Conceptualization.

Declaration of competing interest

The authors declare that they have no known competing financial interests or personal relationships that could have appeared to influence the work reported in this paper.

Acknowledgement

The authors would like to acknowledge Frank Lee for his help with setting up the test heat pump in the psychrometric chambers. The authors would also like to acknowledge the assistance of graduate students Dohyeon Kim and Kia Mossalaei at Herrick Laboratories.

References

[1] Bruce Harley, Mark Alatorre, Christopher Dymond, and Gary Hamer. Csa exp07: Ongoing progress, lessons learned, and future work in load-based testing of residential heat pumps. *International Refrigeration and Air Conditioning Conference*, Paper 2477, 2022.

[2] AHRI. *AHRI Standard 210/240-2024 (I-P): Performance Rating of Unitary Air-Conditioning & Air-Source Heat Pump Equipment.* Air-Conditioning, Heating, and Refrigeration Institute (AHRI), Arlington, VA, USA, 2024.

[3] ASHRAE. *ANSI/ASHRAE Standard 37-2024: Methods of Testing for Rating Electrically Driven Unitary Air-Conditioning and Heat Pump Equipment*. American Society of Heating, Refrigerating and Air-Conditioning Engineers, Atlanta, GA, USA, 2024.

[4] ASHRAE. *ANSI/ASHRAE Standard 116-2010: Methods of Testing for Rating Seasonal Efficiency of Unitary Air Conditioners and Heat Pumps*. American Society of Heating, Refrigerating and Air-Conditioning Engineers, Atlanta, GA, USA, 2010.

[5] BSI. *BS EN 14825:2022: Air Conditioners, Liquid Chilling Packages and Heat Pumps, with Electrically Driven Compressors, for Space Heating and Cooling, Commercial and Process Cooling. Testing and Rating at Part Load Conditions and Calculation of Seasonal Performance*. British Standards Institution (BSI), London, UK, 2022.

[6] JSA. *JIS C 9612:2018: Room Air Conditioners – Testing and Rating for Performance*. Japanese Standards Association, Tokyo, Japan, 2018.

[7] Parveen Dhillon, Drew Welch, Brian Butler, W Travis Horton, and James E Braun. Validation of load based testing methodology for residential air conditioners and heat pumps. *Energy and Buildings*, 299:113607, 2023.

[8] BAM. *Proposal for the Revision of the Harmonised Test Standard EN 14825:2016*. Federal Institute for Materials Research and Testing (BAM), Berlin, Germany, 2019.

[9] U.S. Department of Energy. Energy conservation program: Test procedure for central air conditioners and heat pumps; final rule. Federal Register, 10 CFR Parts 429 and 430, Docket No. EERE-2022-BT-TP-0028, RIN 1904-AF49, 2025. Available at: ://www.govinfo.gov/content/pkg/FR-2025-01-07/pdf/2024-30852.pdf.

[10] Lorenzo Cremaschi and Pedro Perez Paez. Experimental feasibility study of a new load-based method of testing for light commercial unitary heating, ventilation, and air conditioning (ashrae rp-1608). *Science and Technology for the Built Environment*, 23(7):1178–1188, 2017.

[11] Carsten Palkowski, Andreas Zottl, Ivan Malenkovic, and Anne Simo. Fixing efficiency values by unfixing compressor speed: Dynamic test method for heat pumps. *Energies*, 12(6):1045, 2019.

[12] Carsten Palkowski, Stefan von Schwarzenberg, and Anne Simo. Seasonal cooling performance of air conditioners: The importance of independent test procedures used for meps and labels. *International Journal of Refrigeration*, 104:417–425, 2019.

[13] Akash Patil, Andrew L Hjortland, Li Cheng, Parveen Dhillon, James E Braun, and W Travis Horton. Load-based testing to characterize the performance of variable-speed equipment. *International Refrigeration and Air Conditioning Conference*, Paper 2709, 2018.

[14] Andrew L Hjortland and James E Braun. Load-based testing methodology for fixed-speed and variable-speed unitary air conditioning equipment. *Science and Technology for the Built Environment*, 25(2):233–244, 2019.

[15] Jie Ma, Parveen Dhillon, W Travis Horton, and James E Braun. Heat-pump control design performance evaluation using load-based testing. *International Refrigeration and Air Conditioning Conference*, Paper 2520, 2021.

[16] Niccolo Giannetti, Shun Matsui, Ryohei Mori, Jongsoo Jeong, Hifni Mukhtar Ariyadi, Yoichi Miyaoka, Eisuke Togashi, and Kiyoshi Saito. Emulator-type load-based tests for dynamic performance characterization of air conditioners. *Energy and Buildings*, 273:112411, 2022.

[17] CSA. *CSA SPE-07:23 Load-based and climate-specific testing and rating procedures for heat pumps and air conditioners*. Canadian Standards Association (CSA Group), Toronto, Canada, 2023.

[18] Li Cheng, Parveen Dhillon, W Travis Horton, and James E Braun. Automated laboratory load-based testing and performance rating of residential cooling equipment. *International Journal of Refrigeration*, 123:124–137, 2021.

[19] Parveen Dhillon, Li Cheng, W Travis Horton, and James E Braun. Laboratory load-based testing and performance rating of residential heat

pumps in heating mode. *Science and Technology for the Built Environment*, 29(1):49–64, 2023.

[20] Parveen Dhillon, W Travis Horton, and James E Braun. Comparisons of load-based and ahri 210/240 testing and rating for residential heat pumps. *Science and Technology for the Built Environment*, 29(5):473–490, 2023.

[21] U.S. Department of Energy. Energy conservation program: Test procedure for central air conditioners and heat pumps; notice of proposed rulemaking. Federal Register, 10 CFR Parts 429 and 430, Docket No. EERE-2022-BT-TP-0028, RIN 1904-AF49, 2024. Available at: `https://www.energy.gov/sites/default/files/2024-02/cac_tp_nopr.pdf`.

[22] AHRI. *AHRI Standard 1600-2024 (I-P): Performance Rating of Unitary Air-Conditioning and Air-Source Heat Pump Equipment*. Air-Conditioning, Heating, and Refrigeration Institute, Arlington, VA, USA, 2024.

[23] Parveen Dhillon and Dohyeon Kim. Repeatability assessment of load-based testing methodology for residential air conditioning equipment. *ASHRAE Transactions*, 128:287–295, 2022.

[24] Niccolo Giannetti, A Mizuno, Y Miyaoka, Y Sei, K Enoki, K Saito, et al. Feed-forward compensation for emulator-type testing facilities. *International Journal of Refrigeration*, 167:257–268, 2024.

[25] D Dondini, N Giannetti, A Mizuno, Yoichi Miyaoka, and Kiyoshi Saito. Reproducibility assessment of an emulator-type load-based testing methodology. *International Journal of Refrigeration*, 159:39–49, 2024.

[26] S Kia Mossalaei, Jie Ma, Cai Jie W. Travis Horton Dhillon, Parveen, and James Braun. Laboratory evaluation of control verification procedures for certification of variable-speed heat pumps. *ASHRAE Annual Conference*, 2025.

[27] Haopeng Liu, Jie Cai, and Donghun Kim. A hierarchical gray-box dynamic modeling methodology for direct-expansion cooling systems to support control stability analysis. *International Journal of Refrigeration*, 133:191–200, 2022.

[28] Chibuoke Eneh, Jie Ma, James E Braun, W Travis Horton, and Jie Cai. Control performance analysis of load-based testing for air-conditioning and heat pump systems: Part ii - control analysis, design, and validation. *Energy and Buildings*, 2025. submitted.

[29] MathWorks, Inc. *ocr: Optical Character Recognition*, 2024. Computer Vision Toolbox, MATLAB R2024a.

[30] Orkan Kurtulus, Christian K Bach, Romit Maulik, Omer San, Davide Ziviani, Craig R Bradshaw, and Eckhard A Groll. Psychrometric performance testing for hvac&r components and equipment. pages 215–238, 2020.

[31] Li Cheng, James E Braun, and W Travis Horton. Load-based testing using a thermostat environment emulator. *International Journal of Refrigeration*, 126:109–122, 2021.

[32] Dohyeon Kim, Parveen Dhillon, W Travis Horton, and James E Braun. An improved thermostat environment emulator (tee) for load-based testing. *International Refrigeration and Air Conditioning Conference*, Paper 2599, 2024.